IIETA International Information and Engineering Technology Association
Advancing the World of Information and Engineering

Journal Européen des Systèmes Automatisés
Vol. 58, No. 1, January, 2025, pp. 1-12
Journal homepage: http://iieta.org/journals/jesa

Three-Level Boost Converter with Fuzzy Logic for PV-Battery Energy Systems in DC Voltage Control

Ahmed Bahri[1*], Karima Benamrane[2], Thameur Abdelkrim[2], Mohcene Bechouat[3], Nabil Mezhoud[4], Bilel Ayachi[4]

[1] Materials, Energy Systems Technology and Environment Laboratory, Faculté des Sciences et de la Technologie, Université de Ghardaia, Noumerat 47014, Algeria
[2] Unité de Recherche Appliquée en Energies Renouvelables (URAER), Centre de Développement des Energies Renouvelables (CDER), Ghardaïa 47133, Algeria
[3] Laboratoire des Télécommunications, Faculté des Sciences et de la Technologie, Université 8 Mai 1945 Guelma Université de Ghardaia, Noumerat 47014, Algeria
[4] Electrical Engineering Department, LES Laboratory, Faculty of Technology, University of 20 August 1955-Skikda, El Hedaiek 21015, Algeria

Corresponding Author Email: bahri.ahmed@univ-ghardaia.edu.dz

https://doi.org/10.18280/jesa.580101

Received: 9 September 2024
Revised: 8 January 2025
Accepted: 17 January 2025
Available online: 31 January 2025

Keywords:
photovoltaic system, three-level boost, three-level inverter NPC, FPID, DC link voltage

ABSTRACT

This research presents a unique configuration to enhance the efficiency of a hybrid photovoltaic-battery energy system. The system combines a fuzzy logic PID controller to control the DC bus voltage with a three-level inverter (3LI) and three-level boost converter (3LBC) to achieve optimal energy consumption. To achieve maximum power extraction from the solar generator and maintain capacitor voltage balancing, a double-loop control system employs a perturbation and observation (P&O) algorithm for maximum power point tracking (MPPT) and proportional integral (PI) regulators. Furthermore, a three-level inverter NPC guarantees effective power transmission to the AC load. In the event of a power imbalance due to fluctuations in solar radiation or an AC load, a buck-boost converter (BBC) facilitates bidirectional energy transfer between the DC connection and the battery energy storage (BES). The PID controller uses a fuzzy logic controller (FLC) to determine its parameters. The study shows that using simulations on the MATLAB/SIMULINK platform to test the 3LBC and the fuzzy PID (FPID) controller can get rid of total harmonic distortion (THD) and improve system performance.

1. INTRODUCTION

Due to its potential to improve energy sustainability and grid stability, the integration of renewable energy sources, especially photovoltaic (PV) systems, with energy storage systems (ESS), such as batteries, has gained significant interest recently [1]. In these hybrid energy systems, efficient energy conversion and management are critical to achieving maximum resource utilization and overall system performance [2]. The boost converter, which is essential to these systems, controls voltage levels and maximizes power extraction from the PV array [3]. However, typical boost converters may restrict the efficiency, accuracy of control, and flexibility to operate in dynamic environments.

Numerous studies [4-7] have explored the use of three-level boost converters in photovoltaic systems, aiming to address these limitations. These investigations have proposed novel topologies and evaluated the performance of such converters for (MPPT) and grid integration. Results have shown improved efficiency, better voltage regulation, and reduced harmonic distortion compared to traditional converters.

Moreover, the integration of energy storage systems further enhances system capabilities by intelligently managing surplus power during periods of excess energy generation and utilizing stored energy during low generation periods. This mitigates the intermittency of renewable sources and ensures a continuous, stable power supply to the connected load [8].

In connecting photovoltaic systems with energy storage systems to variable loads, the choice of a three-level NPC inverter offers several advantages, including improved voltage quality, reduced harmonic distortion, and enhanced system efficiency. This inverter's three-phase output capability makes it suitable for integration into existing power distribution systems [9, 10].

In stand-alone hybrid energy systems, maintaining stable DC-link voltage is crucial for reliable performance. Various technical control strategies, such as proportional-integral (PI) control [11], fractional order PID (FOPID) [12], sliding mode control [13], and novel SSA-PSO-DSMC control [14], have been developed for effective regulation [15].

Moreover, the contribution of this paper lies in presenting a new configuration for enhancing the performance of hybrid photovoltaic-battery energy systems. By integrating a 3LBC,3LI, and a FPID controller for DC bus voltage, the

system aims to optimize energy utilization. Through simulation on MATLAB/SIMULINK, the study shows that this setup effectively minimizes THD, leading to improved system performance. Furthermore, we present a comprehensive analysis of a proposed configuration for a photovoltaic (PV) system, along with the modeling and control strategies employed. Section 2 outlines the proposed configuration, highlighting its key components and their interconnections. This section offers a detailed overview at the architecture of the hybrid system, detailing the integration of the photovoltaic array, battery storage, and the associated power electronic converters. Subsequently, in Section 3, we delve into the modeling and control techniques tailored specifically for PV systems, elucidating their significance in optimizing performance and efficiency. This section includes mathematical modeling of the PV array and battery storage, as well as the control algorithms implemented to maximize energy harvesting and ensure reliable operation under varying environmental conditions. Additionally, we introduce the 3LB DC-DC converter in Section 4, a critical component within the proposed configuration, and discuss its role in enhancing power conversion efficiency. This section explores the design principles of the 3LBC, its operational benefits, and its impact on reducing switching losses and improving voltage regulation. Section 5 focuses on the implementation of a fuzzy proportional integral derivative (FPID) controller for regulating the DC-link voltage, thereby ensuring stable operation and effective utilization of the PV system. We provide a detailed description of the fuzzy logic-based control strategy, its integration with the PID control mechanism, and the advantages it offers in terms of dynamic response and robustness against parameter variations. In Section 6, we conclude with our findings and explore future research opportunities. This concluding section summarizes the key outcomes of the study, reflects on the performance improvements achieved through the proposed configuration, and suggests directions for further advancements in hybrid PV-battery systems, including potential enhancements in control strategies and converter topologies.

2. PROPOSED CONFIGURATION

The hybrid energy system shown in Figure 1 consists of a 3LBC powered by a PV panel.

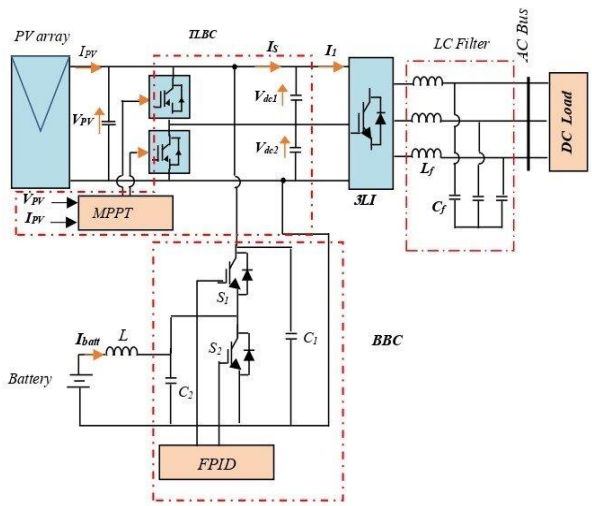

Figure 1. The hybrid energy system

The converter is connected to a battery storage system and utilizes FPID (Fuzzy Proportional-Integral-Derivative) regulators in a buck-boost design. A P&O algorithm combined with a PI controller is used for (MPPT) in the photovoltaic system. 3LI is coupled between a DC-Link and a DC load. The system's objective is to maximize energy efficiency, enhance system stability, and boost overall performance.

3. MODLING AND CONTROL OF PV SYSTEM

This study uses a five-parameter, single-diode model [16] to simulate solar cell output, as shown in Figure 2 [17, 18]. The PV module used is the BP Solar SX 3190, as specified in Table 1 under STC (1000 W/m², 25°C). The PV panel's output power is determined by Eq. (1) [17], and Table 2 lists the five key parameters for the single-diode model under STC. PV power production varies with atmospheric conditions, affecting the curve I/V, which is nonlinear and influenced by solar irradiation, as illustrated in Figure 3(a). Figure 3(b) highlights that the maximum power is achieved at the knee operation point, ensuring PV generator operation at this point is crucial making [19, 20].

$$P_{PV} = N_{PV}.N_P.I_{Ph}.V_{PV} - N_{PV}.N_P.I_0.V_{PV}\left(exp\left(\frac{V_{PV}}{N_S.V_t}+\frac{I_{PV}.R_S}{N_P.V_t}\right)-1\right) - \frac{N_P}{R_P}.V_{PV}.\left(\frac{V_{PV}}{N_S}+\frac{I_{PV}.R_S}{N_P}\right) \quad (1)$$

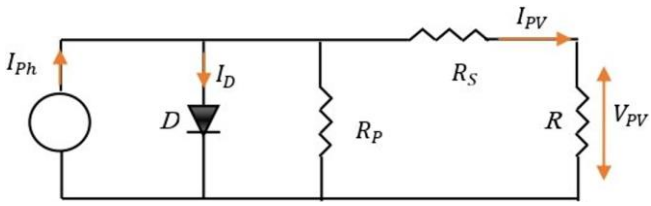

Figure 2. Model of a solar cell with a single diode

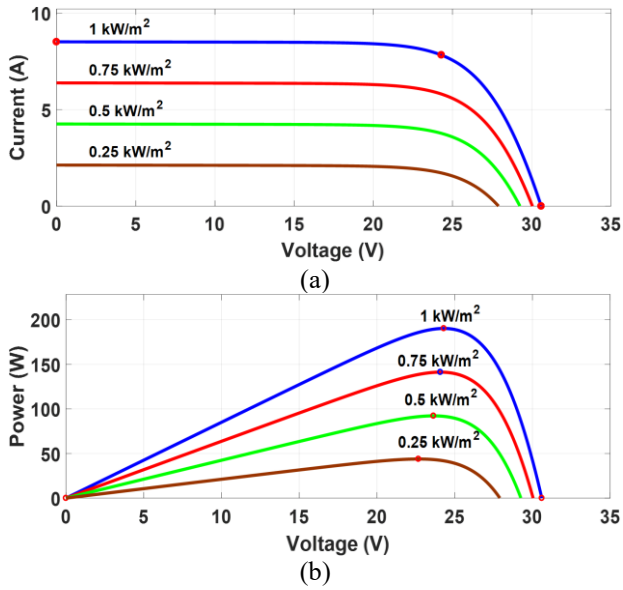

Figure 3. Schematic characteristic of Bp Solar SX3190 module (a) I/V Characteristic, (b) P/V Characteristic

Table 1. The specifications of the Bp Solar SX3190 module

Parameter	Value
Maximum power (P_{MPP})	190.25 W
Maximum power point voltage (V_{MPP})	24.3003 V
Maximum power point current (I_{MPP})	7.82945 A
Open-Circuit voltage (V_{oc})	30.6021 V
Short-Circuit current (I_{sc})	8.51029 A
Number of series-connected modules per string	6
Number of parallel strings	6

Table 2. Model parameters for 1 module

R_s (Ω)	R_p (Ω)	I_{sat} (A)	I_{ph} (A)	Q_d
0.17514	755.51	1.0647×10^{-6}	8.5158	1.5

4. THREE-LEVEL BOOST DC-DC CONVERTER

Boost choppers are frequently employed in energy conversion systems due to their uncomplicated topology and control mechanism [21-23]. The TLBC is particularly advantageous in high-power applications due to reduced switching and reverse recovery losses of the diode. Furthermore, the TLBC can operate with a smaller inductor compared to conventional boost converters as a result of reduced inductor current ripple [23, 24].

4.1 Three level modeling

Figure 4 illustrates the configuration of the three-level boost converter, which consists of two boost converters connected at the midpoint of the transistors (S_{b1}, S_{b2}) and capacitors (C_{d1}, C_{d2}). The transistors are controlled with a shift of $Ts/2$ [4].

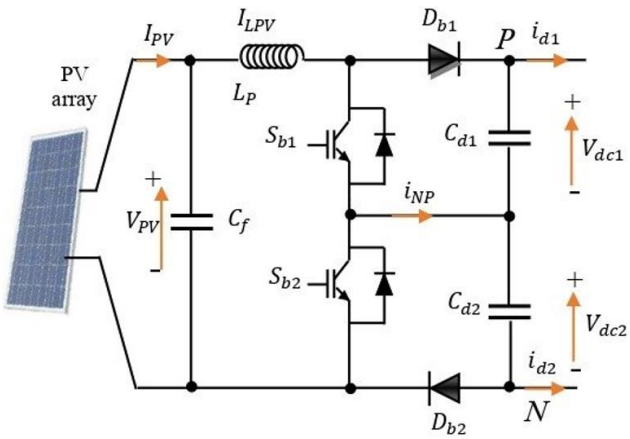

Figure 4. Three-level boost converter

The averaged model can be used to describe how the input voltage V_{PV}, inductance current I_{LPV}, and neutral point current i_{NP} behave dynamically [21, 22].

$$\begin{cases} L_b \dfrac{di_{LPV}}{dt} = V_{PV} - (1-D_1)V_{dc1} - (1-D_2)V_{dc2} \\ C_f \dfrac{dV_{PV}}{dt} = i_{PV} - i_{LPV} \\ i_{NP} = (D_1 - D_2) i_{LPV} \end{cases} \quad (2)$$

D_1: Switch S_{b1} duty cycle.
D_2: Switch S_{b2} duty cycle.

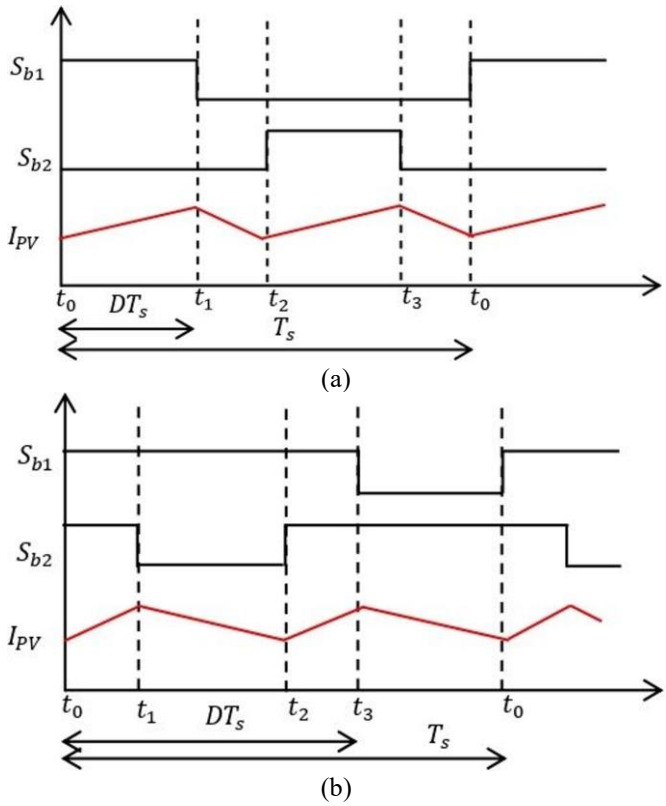

Figure 5. 3LBC waveforms, (a) D<0.5, (b) D>0.5

Figure 5(a) shows the 3LBC waveforms at $D < 0.5$. Prior to t_0, both switches S_{b1} and S_{b2} remain open. At t_0, switch S_{b1} is turned on and the current flows through L_b, S_{b1}, C_{d2}, and D_{b2}. This causes an increase in the current of the PV generator I_{pv} Eq. (3) [21].

$$I_{PV}(t) = I_{PV}(t_0) + \frac{V_{PV} - V_{dc}/2}{L_b}(t - t_0) \quad (3)$$

where,

$$V_{dc} = V_{dc1} + V_{dc2} \quad (4)$$

When time reaches t_1, switches S_{b1} is open, and current flows through L_b, D_{b1}, C_{d1}, C_{d2}, and D_{b2}. Consequently, the PV generator's current, I_{pv}, drops.

$$I_{pv}(t) = I_{pv}(t_1) - \frac{V_{dc} - V_{pv}}{L_b}(t - t_1) \quad (5)$$

During time t_2, when switch S_{b2} is closed, current flows through L_b, D_{b1}, C_{d1} and S_{b2}, leading to an increase in the current of the PV generator I_{pv}. On the other hand, switch S_{b2} is open at time t_3, both switches are open, and current passes through L_b. D_{b1}, C_{d1}, C_{d2}, and D_{b2}, causing a decrease in the current of the PV generator I_{pv} Eq. (5) [21].

Figure 5(b) shows the theoretical waveforms of 3LBC when the duty cycle surpasses 0.5. Prior to time t_0, one of the switches, S_{b1}, is open while the other switch, S_{b2}, is closed. At t_0, S_{b1} is closed, and both switches become conductive. As a result, the current flowing through the PV generator, indicated by Eq. (6) [25].

$$I_{PV}(t) = I_{PV}(t_0) + \frac{V_{PV}}{L_b}(t - t_0) \quad (6)$$

At t_1, S_{b2} is opened, and the current passes through L_b, S_{b1}, C_{d2}, and D_{b2}. As a result, the current flowing through the PV generator (I_{pv}) decreases, as indicated by Eq. (7).

$$I_{PV}(t) = I_{PV}(t_1) - \frac{V_{dc}/_2 - V_{PV}}{L_b}(t - t_1) \quad (7)$$

At t_2, S_{b2} is closed, allowing both switches to conduct the current. As a result, the current flowing through the PV generator (I_{pv}) increases, as indicated by Eq. (6). At t_3, S_{b1} is opened, causing the current to pass through L_b, D_{b1}, C_{d1}, and S_{b2}. This, in turn, causes a decrease in the current flowing through the PV generator (I_{pv}), denoted by Eq. (7) [21].

4.2 Proposed MPPT

The P&O method, also known as Perturbation and Observation, is widely used to maximize photovoltaic power and balance capacitor voltages by tracking the maximum power point (MPPT) of PV systems. This technique adapts to changes in solar irradiance, as discussed in sources [26-28].

4.3 Voltage balance control

Capacitors C_{d1} and C_{d2} are alternately charged to voltages V_{dc1} and V_{dc2}. Despite having the same capacitance, a voltage imbalance arises due to differences in real capacitors and their equivalent series resistance. A voltage balancing controller is required to equalize the capacitor voltages by adjusting the duty cycle, as shown in Figure 6. S_{b1} and S_{b2} are the gate pulses for the switches. In the 3LBC DC-DC converters, the duty ratio determines the input-output voltage relationship.

$$\frac{V_{dc}}{V_{PV}} = \frac{1}{1 - 0.5D_1 - 0.5D_2} \quad (8)$$

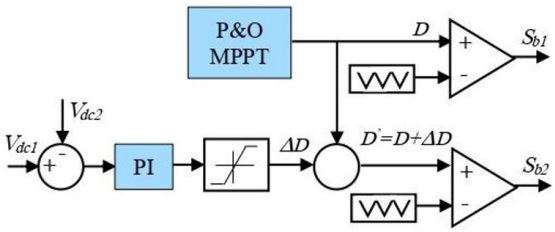

Figure 6. Block diagram of MPPT with voltage balance control

If D_1=D_2=D, then

$$\frac{V_{dc}}{V_{PV}} = \frac{1}{1 - D} \quad (9)$$

V_{PV} voltage from the PV fluctuates with environmental changes. The MPPT control determines the duty cycle (D) for boost switch S_{b1}, while S_{b2} duty cycle is controlled by an additional PI controller, which adjusts (D') based on the voltage error ($V_{dc1} - V_{dc2}$).

Consider

$$\Delta D = K_p + \frac{K_i}{s}(V_{dc1} - V_{dc2}) \quad (10)$$

The transfer function of the PI controller is represented by $K_p + \frac{K_i}{s}$. The duty cycle $D' = D + \Delta D$ is used to operate switch S_{b2} in the converter in order to equalize the voltage across the capacitors.

Imbalanced capacitor voltages can lead to uneven distribution of power, resulting in increased switching and conduction losses in the converter, thereby reducing overall efficiency.

5. BATTERY MODELING

Energy storage devices like batteries enhance the reliability and efficiency of power distribution [29]. This study uses an equivalent circuit model with V and internal resistance R in series [30], allowing the battery's output voltage to be expressed as:

$$V_{bat} = V - RI_{bat} \quad (11)$$

The battery voltage Vbat (V) and current Ibat (A) are greatly affected by internal resistance, temperature and factors like State of Charge (SOC). Figure 7 shows the battery's electrical model.

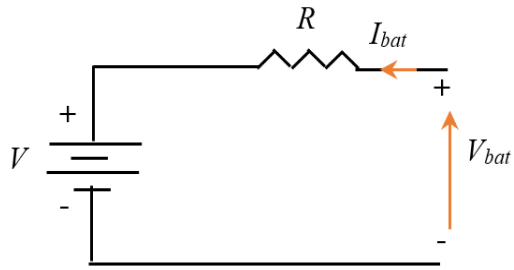

Figure 7. The standard battery models

This study employs a basic battery model for energy management, where the (SOC) depends on time, production sources, and charge variation, as defined by equation [31]:

$$SOC(t) = \begin{cases} SOC(t - \Delta t) + P_{bat}\dfrac{\eta_{ch}}{C_n V_{dc}}\Delta t \\ SOC(t - \Delta t) + P_{bat}\dfrac{1}{\eta_{dis} C_n V_{dc}}\Delta t \end{cases} \quad (12)$$

Δt is the time step, P_{bat} the battery power, C_n the nominal capacity, η_{ch} and η_{dis} are the charging/discharging efficiencies, and V_{dc} the nominal DC voltage.

The battery acts as an essential link between the PV system and the load, operating in two modes: charging and discharging. The Buck-Boost Controller (BBC), using two switches Q_1 and Q_2, regulates the DC voltage to maintain the required level and manages the battery's charge and discharge based on the PV panel's output.

In this study, the battery bank receives the excess power before it surpasses its maximum storage capacity as a result of high power situations [32]. The flow chart in Figure 8 illustrates how the battery and photovoltaic system coordinate control. The battery's lower and higher state of charge restrictions range between 0.2 and 0.8 [17].

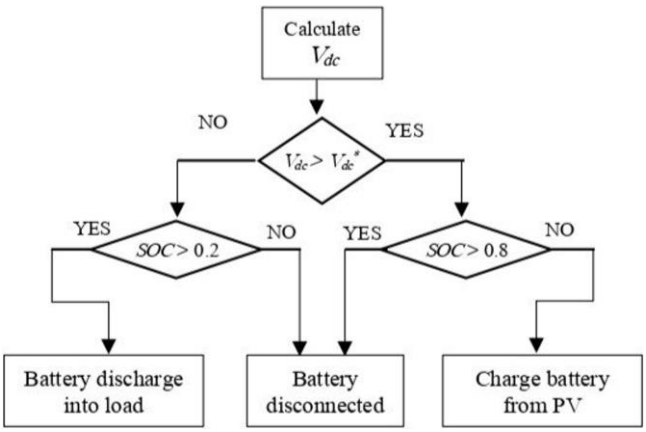

Figure 8. Algorithm for controlling DC link voltage

6. THREE LEVELS INVERTER NPC MODLING AND CONTROL

The three-level (NPC) inverter as illustrated in Figure 9 consists of two DC voltage sources and three arms. Each arm contains four bidirectional current-controlled switches and two midpoint diodes to achieve zero-level output voltage. Controllable switches manage the inverter's turn-on and turn-off operations.

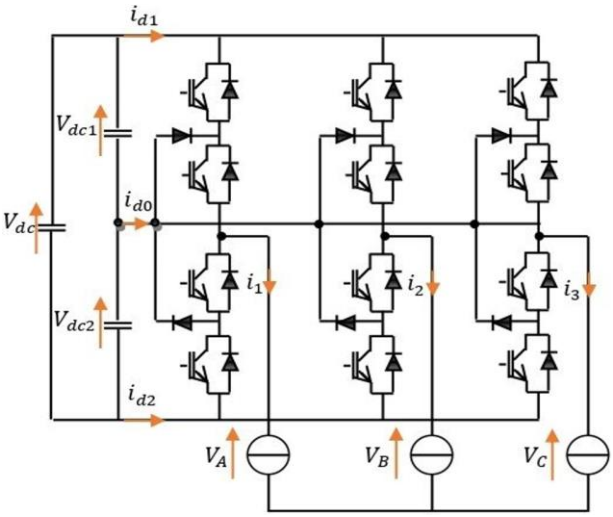

Figure 9. Three-level three-phase inverter with NPC configuration

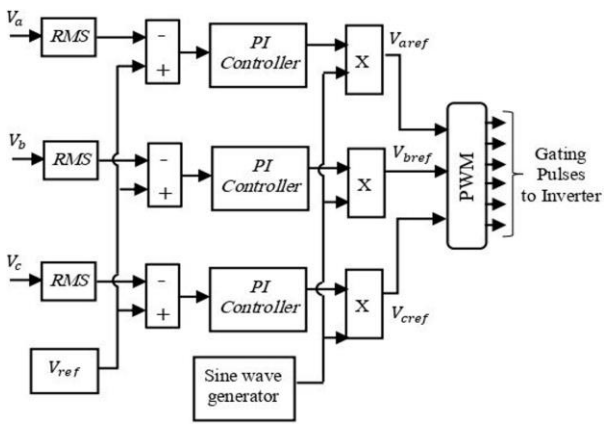

Figure 10. PWM control of a three-level inverter

A three-phase load-side inverter provides stable voltage and frequency [12]. In distribution systems, unbalanced single-phase loads create phase current differences and voltage imbalances. To regulate the load voltage, a voltage vector adjustment feeds the error between the RMS phase voltages and the reference voltage into a PI controller, as shown in Figure 10. The controller multiplies the output by a unit sine wave generator to obtain the reference phase voltages (V_{aref}, V_{bref}, V_{cref}) for generating PWM pulses for the inverter [17].

7. FPID CONTROLLER of $V_{dc\text{-}link}$ VOLTAGE

Fuzzy theory translates complex processes and natural language into machine-readable format. Based on fuzzy logic, it excels in controlling nonlinear systems by leveraging cognitive processes and practical knowledge [33]. A fuzzy control system includes a fuzzy controller and a plant, as shown in Figure 11.

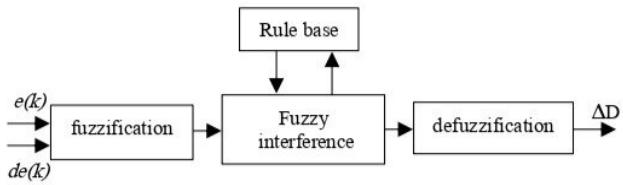

Figure 11. Architecture of a fuzzy control system

A fuzzy controller comprises fuzzification, a rule base, fuzzy inference, and defuzzification. Fuzzification maps input values to language descriptions, while the rule base mimics human cognition using if-then rules [33]. Fuzzy inference generates control values from input values, membership functions (MFs), and rules. Defuzzification then converts the fuzzy control value into the plant's control value [33]. A fuzzy PID (FPID) is designed to maintain DC link voltage stability.

Four basic blocks define the FPID controller. Fuzzification turns real-valued variables into fuzzy sets, which fuzzy logic systems utilize to control output variables. DC bus voltage (V_{bus}) is checked continually. The fuzzy logic controller will receive the error *e(k)*, the difference between the V_{bus} voltage and the reference voltage V_{ref}, and its rate of change, *de(k)*, at sampling moment *k*. The fuzzy logic controller will decide the output variable, ΔD.

As stated earlier, the FLC necessitates numerous inputs. Therefore, it is necessary to carefully choose and clearly specify the inputs in the first place. In this study, the *e(k)* and *de(k)* are regarded as inputs, while the change in duty cycle ΔD is considered as the output of the FPID system.

The FLC needs several inputs. Therefore, inputs must be carefully selected and properly defined. This research uses *e(k)* and *de(k)* as inputs and ΔD as the output of the FPID system. The *e(k)*, *de(k)*, and ΔD are defined as follows:

$$\begin{aligned} e(k) &= V_{ref} - V_{bus}(k) \\ de(k) &= e(k) - e(k-1) \end{aligned} \tag{13}$$

This study utilizes various linguistic characteristics, with specific details provided in Table 3 [34].

The (FLC) utilizes the following IF-THEN rules, mapping the inputs *e(k)* and *de(k)* to the output (ΔD):

IF *e(k)* is Negative Big (NB) AND *de(k)* is Negative Big

(NB), THEN Δ*D* is Negative Big (NB).

IF *e(k)* is Negative Medium (NM) AND *de(k)* is Negative Medium (NM), THEN Δ*D* is Negative Medium (NM).

IF *e(k)* is Negative Small (NS) AND *de(k)* is Negative Small (NS), THEN Δ*D* is Negative Small (NS).

IF *e(k)* is Zero (ZE) AND *de(k)* is Zero (ZE), THEN Δ*D* is Zero (ZE).

IF *e(k)* is Positive Small (PS) AND *de(k)* is Positive Small (PS), THEN Δ*D* is Positive Small (PS).

IF *e(k)* is Positive Medium (PM) AND *de(k)* is Positive Medium (PM), THEN Δ*D* is Positive Medium (PM).

IF *e(k)* is Positive Big (PB) AND *de(k)* is Positive Big (PB), THEN Δ*D* is Positive Big (PB).

Table 3. Fuzzy adaptive rules

Error *e(k)*	Change of Error *de(k)*	Change in Duty Cycle (Δ*D*)
NB	NB	NB
NM	NM	NM
NS	NS	NS
ZE	ZE	ZE
PS	PS	PS
PM	PM	PM
PB	PB	PB

There are other (MFs) described in literature, however the Trapezium technique is chosen as the most optimal based on its past performance and expert knowledge [35].

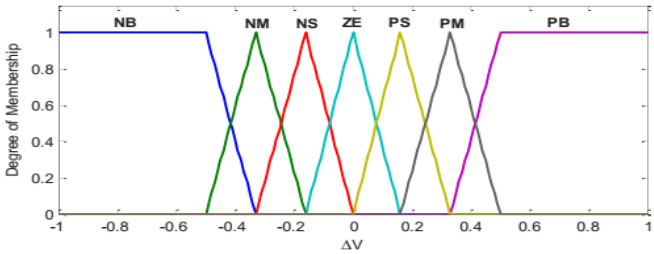

Figure 12. MF for input variable *e(k)*

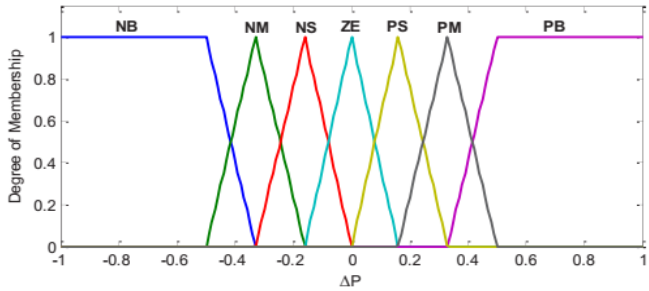

Figure 13. MF for input variable d*e(k)*

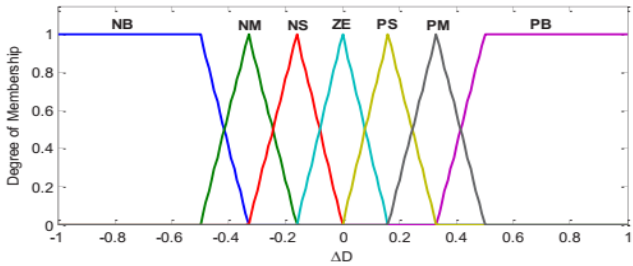

Figure 14. MF for output variable Δ*D*

The (MFs) for the de(k) and e(k) input variables are displayed in Figures 12 and 13, respectively. Figure 14 shows the (MFs) for the output variable ΔD. The main purpose of the proposed guidelines is to adjust the bidirectional converter duty ratio to maintain the DC link voltage near the reference. The defuzzification block controls the bus voltage by generating the desired output value, ΔD. The Center of Area (COA) method is commonly used for defuzzification, where the fuzzy centroid is calculated by integrating the inference results. Eq. (14) determines the output D by multiplying the center points of the output (MFs) by their weights and summing them up [36, 37].

$$D = \frac{\sum_{j=1}^{k} D_j \mu_A(D_j)}{\sum_{j=1}^{k} \mu_A(D_j)} \tag{14}$$

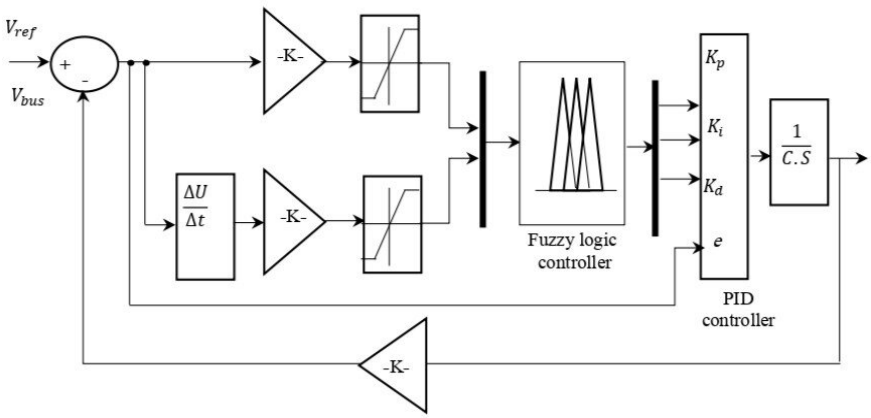

Figure 15. Structure of FPID controller

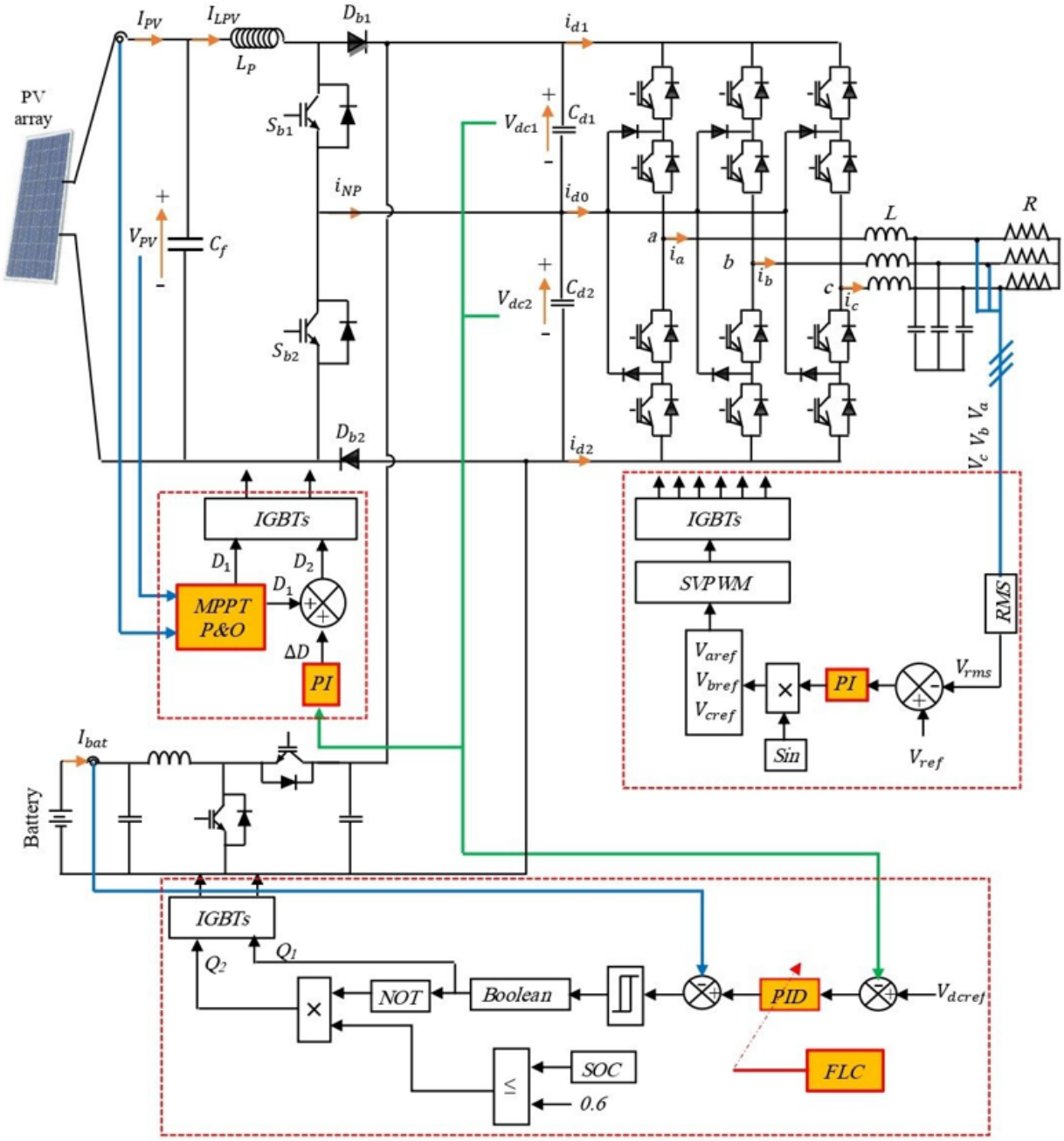

Figure 16. The proposed block PV/Battery

In this context, D represents the crisp output value, D_j stands for the max-min composition center at the output (MFs), where $\mu A(D_j)$ is the j_{th} membership function's peak value, and D_j denotes the j_{th} input value. According to study, MOSFET gates should get the duty ratio value with the crisp value D. However, in this study, the crisp value D is directly transferred to the gate of IGBTs without undergoing this process, and the Fuzzy Logic Controller (FLC) functions effectively in this setup.

The Simulink model used to obtain the system's responses is shown in Figure 15. The FPID controller output, representing the duty ratio variation $\Delta D(k)$, is added to the previous duty ratio $D(k\text{-}1)$ to calculate the final output $D(k)$ as per [36].

$$D(k) = D(k-1) + \Delta D(k) \tag{15}$$

The proposed PV/Battery system is connected to the three-level inverter to supply power to three-phase loads through a DC link voltage, as shown in Figure 16.

8. SIMULATION RESULTS AND DISCUSSION

The control strategy for the PV/Battery converse on system using a 3LBC and 3LI with storage, as illustrated in Figure 16, comprises:

- An MPPT P&O controller and another PI controller are used for 3LBC for maximum power extraction and bus voltage balancing.
- An SVPWM block for precise control of the three-level inverter.
- A FPID regulator associated with the battery management algorithm to control the buck-boost converter.

For the following factors, simulation results are given:

- The inverter's switching frequency is 2.5 kHz.

• Boost converter switching frequency is 18 kHz
• Output effective voltage: V_{eff} = 220V
• DC bus reference voltage: V_{dcref} = 600V

To test the performance of the proposed control and extract the maximum power from the photovoltaic generator, we initiated the simulation at t=0 S with radiation at 1000W/m^2. Subsequently, from t=1S to t=3S, the radiation decreased to 500W/m^2. It then increased again to 700W/m^2 between t=3S and 5S. Finally, it stabilized at a value of 1000W/m^2 between t=5S and 6S Figure 17. The temperature remained constant at T=25°C.

Figure 18 displays the in power load transition from 6000 W to 8000 W occurring between 2 and 3 seconds. This is carried out in order to assess the controller's resilience.

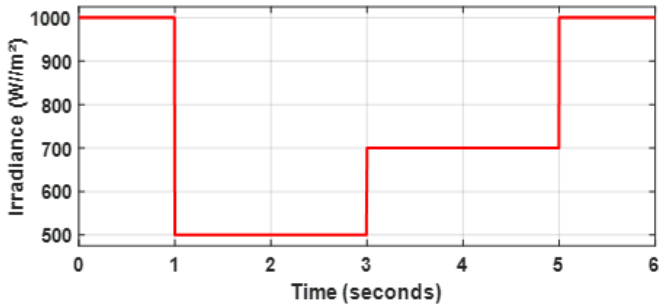

Figure 17. Variation of irradiance

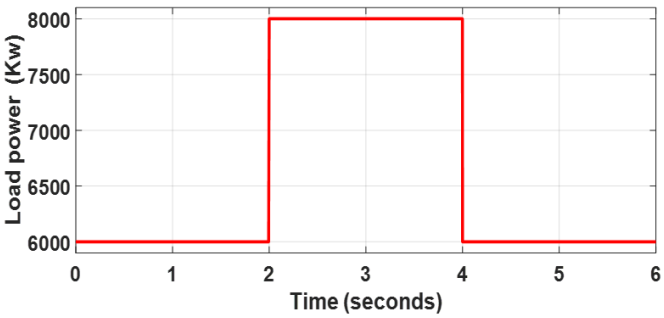

Figure 18. Variation of load

Figure 19 and Figure 20 serve as crucial visual aids in understanding the performance of the photovoltaic (PV) system under different control schemes. In Figure 19, the voltage V_{pv} and current I_{pv} characteristics of the PV generator are meticulously illustrated, providing insights into its behavior under varying conditions. Meanwhile, Figure 20 delves deeper into the system's power output, presenting comparative analyses between two prominent converter configurations: the two-level and three-level converters.

Notably, the pivotal point of maximum power output, where the voltage reaches 200V and the current 40A, highlights the system's efficiency, yielding an impressive 8000W of power. This observation underscores the successful operation of the Maximum Power Point Tracking (MPPT) algorithm, crucial for optimizing the PV system's performance.

However, the comparison between the two-level and three-level converter systems reveals nuanced differences. While both employ MPPT control algorithms, the integration of proportional integral (PI) regulators in the three-level boost control system enhances its stability. This enhancement is particularly evident in the power generation process, where the three-level converter system demonstrates superior stability compared to its two-level counterpart.

This finding suggests that the incorporation of (PI) regulators contributes to better control over the power generation process, mitigating potential fluctuations and ensuring consistent performance. As such, it underscores the significance of advanced control strategies in enhancing the overall efficiency and reliability of PV systems, offering valuable insights for future design and optimization endeavors.

Figure 21 illustrates the power difference between the (3LBC) and the Two-Level Boost Converter (2LBC). The 3LBC delivers 200 W more power than the 2LBC, representing a 2.5% improvement in efficiency. This highlights the advantage of the (3LBC) in achieving higher power output and better performance for high-demand applications.

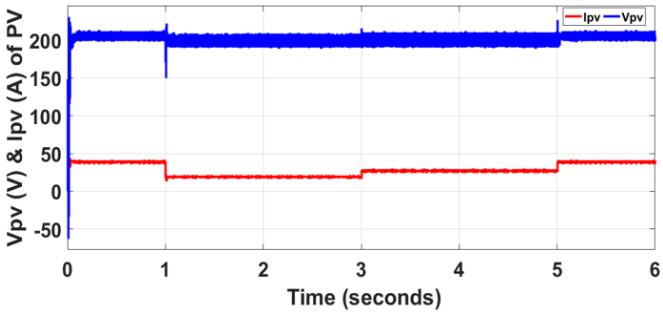

Figure 19. Voltage and current of PV panel

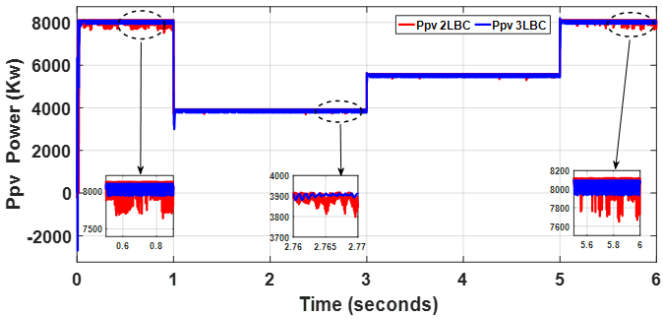

Figure 20. Power of PV

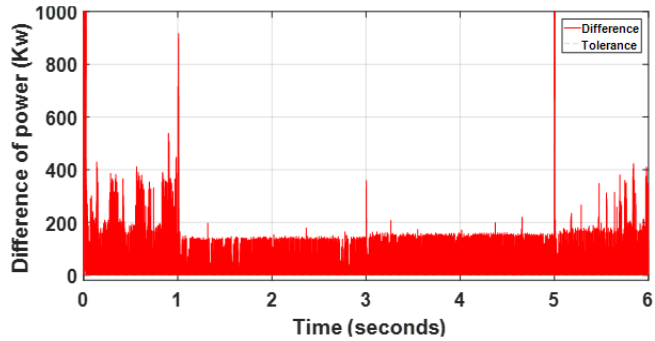

Figure 21. Difference of power with 3LBC and 2LBC

This notable variance in power output underscores the efficacy of the three-level boost converter over its two-level counterpart. The observed superiority of the three-level configuration suggests that it possesses inherent advantages or optimizations that enable it to extract more power from the photovoltaic system compared to the two-level converter.

The implications of this finding are profound, as they highlight the importance of selecting the appropriate converter

topology for maximizing power extraction efficiency in photovoltaic systems. By demonstrating the superiority of the three-level boost converter, Figure 21 provides valuable insights for system designers and engineers, directing them towards more effective and efficient solutions for harnessing solar energy.

In conclusion, the clear difference in power output showcased in Figure 21 unequivocally favors the utilization of a three-level boost converter over a two-level counterpart, reaffirming its status as the superior choice for enhancing the performance and productivity of photovoltaic systems.

The evaluation of the proposed controller aimed at maximizing power extraction from the photovoltaic generator under varying conditions of irradiance and load. With a fixed DC link voltage set at 600V, the comparative analysis between the FPID controller and the traditional PID controller was conducted. Figure 22 serves as a clear visual representation of this evaluation, showcasing the voltage and control responses of the DC link. Notably, the results unmistakably demonstrate the superiority of the FPID controller over the PID controller. The FPID controller exhibits several advantages, including quicker and smoother response to DC link voltage variations, reduced sensitivity to fluctuations in load power, and its ability to eliminate oscillations in steady-state electrical power. These studies demonstrate FPID controller efficacy in optimizing the performance of the photovoltaic system, offering enhanced stability and efficiency in power extraction.

Figure 23 demonstrates a significant difference of up to 12.04 V between the performance of FPID and PID controllers, providing clear evidence of the superiority of the FPID controller. This disparity underscores the enhanced precision and effectiveness of FPID control in comparison to PID control, advocating for its adoption in applications where precise control and optimization are crucial.

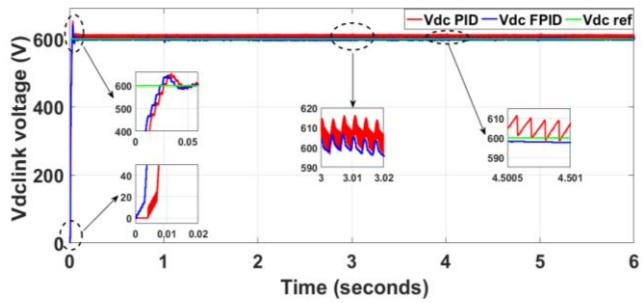

Figure 22. DC bus voltage

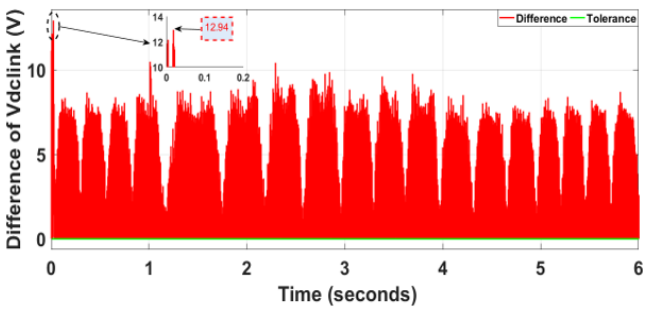

Figure 23. Difference of V_{dc} link

The 3LBC is designed to achieve not only maximum power extraction from the photovoltaic generator but also to maintain voltage equality between V_{dc1} and V_{dc2} through its control mechanism. Figure 24 shows that 3LBC output voltages are equal.

Furthermore, Figure 25 demonstrates the excellent performance of the BBC controller, as it effectively manages battery bank power variations (charging/discharging) to maintain system power balance across various scenarios of load and irradiance. In practice, when the power of AC load exceeds the generated PV power, the BBC controller discharges battery power to supply the AC load. On the other hand, if the load power is less than the PV power output, it can also charge the battery.

Figure 26 illustrates the (SOC), which starts at 60% and increases until 1 s while charging. The discharge phase is limited to 5 s, occurring when there is low PV power and high power demand. Following this, the battery undergoes recharging if the PV power rises and power consumption decreases.

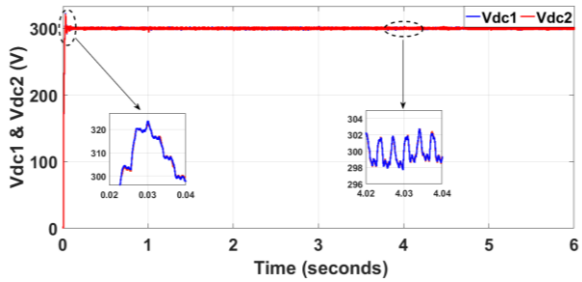

Figure 24. DC bus voltages V_{dc1} & V_{dc2}

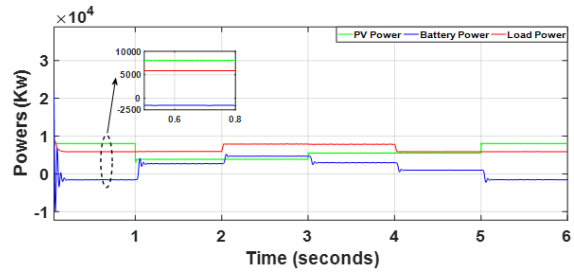

Figure 25. Power distribution for photovoltaics, batteries, and load

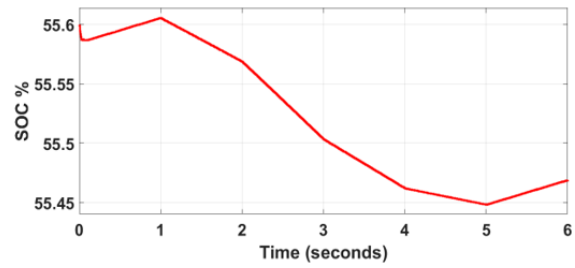

Figure 26. Battery SOC

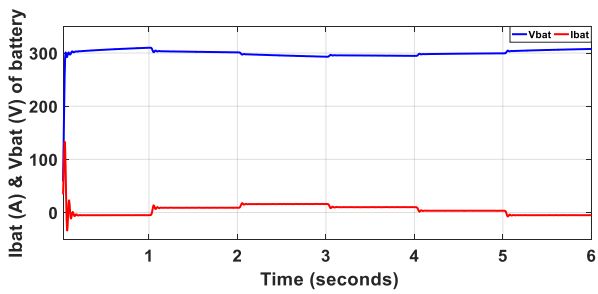

Figure 27. Current and voltage of battery

Figure 27 shows the curve of battery voltage and current, providing a visual representation of both the charging and discharging processes of the battery, which can be observed from the current curve.

Figures 28 and 29 show the voltage and current waveforms of the three-level inverter under FPID control. This result demonstrates the enhanced quality of the power supplied and the efficacy of the suggested 3LI control system.

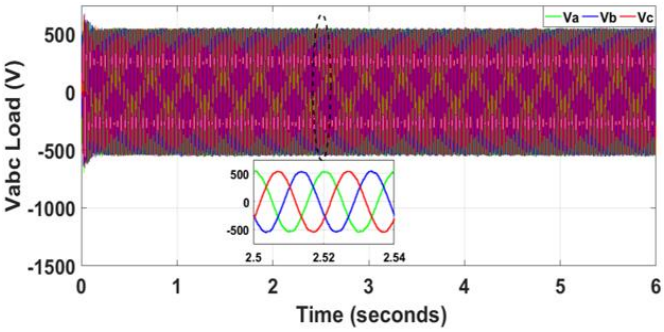

Figure 28. Output voltage of load

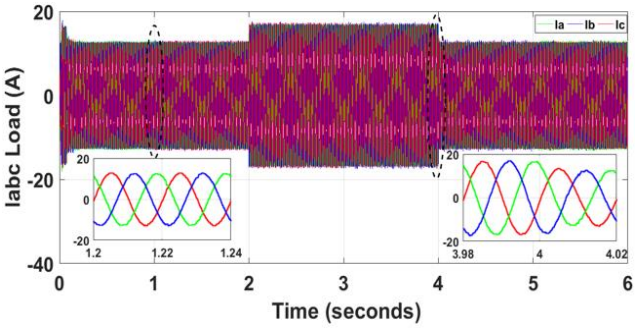

Figure 29. Output current of load

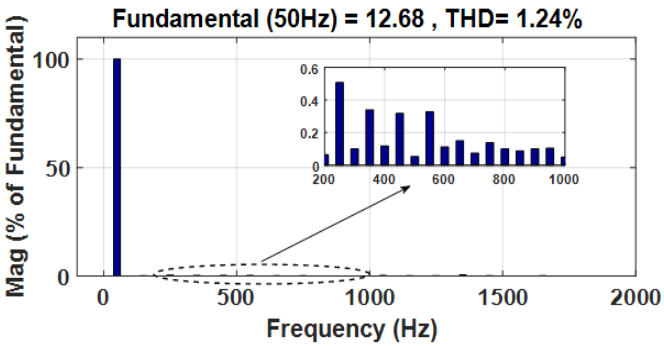

Figure 30. Spectrum analysis of current I_a

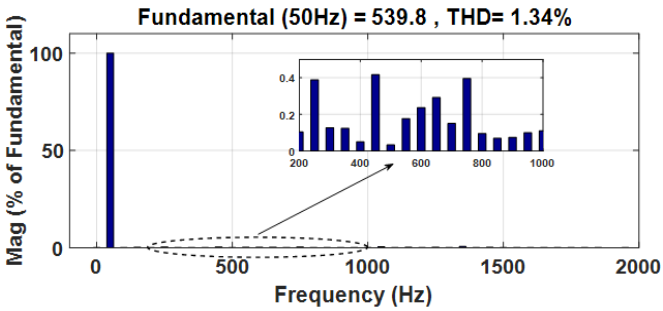

Figure 31. Spectrum analysis of voltage V_a

To verify the quality of the NPC inverter's current and voltage outputs under the suggested control, THD was determined to be less than 5%, with values of 1.24% and 1.34% for current and voltage, respectively Figure 30 and Figure 31. This result is exemplary compared to the THD values reported in several other references.

A comparative analysis in this section highlights the FPID's advantages, as shown in Table 4.

Table 4. Comparison of the proposed strategy

Ref.	System Elements	Type of Converter	Controller	THD
[31]	Wind PV and battery residential load	boost converter	PI	3.68%
[38]	PV and battery rural area application	boost converter	PI	3.98%
[17]	PV and battery loads	boost converter	TID	1.74%
[39]	PV and battery grid connected	boost converter	PI	3.30%
[40]	PV and battery grid connected	boost converter	Fractional Order PID	4.18%
Proposed strategy	PV and battery loads	Three-level boost converter	FPID	1.24%

9. CONCLUSION

This paper presents a novel (3LBC) design integrated with a fuzzy logic controller to manage the DC bus voltage in a photovoltaic-battery energy system. The results demonstrate the considerable benefits that the 3LBC offers in terms of power extraction quality from photovoltaic panels when compared to its two-level equivalent (2LBC). Specifically, the three-level design significantly enhances the power conversion efficiency and reduces the overall losses, leading to improved energy harvesting from the PV panels. Furthermore, the simulation results for the P&O method of the MPPT algorithm are encouraging. The 3LBC effectively supports the P&O algorithm, ensuring that the PV system operates consistently at its maximum power point, thereby optimizing energy output. In the three-level inverter (3LI), a PI controller can regulate voltage balance between V_{dc1} and V_{dc2} in the 3LBC. However, the FPID controller proves superior in maintaining the stability of the V_{dc} link voltage. The FPID controller's advanced tuning capabilities and adaptability result in more precise voltage regulation and enhanced system stability, particularly under dynamic load conditions. When connected to the battery, a buck-boost converter handles potential power imbalances and ensures that energy is transferred bidirectionally with minimal THD. This bidirectional capability is crucial for efficient energy storage and retrieval, allowing the system to balance supply and demand effectively. The neutral-point-clamped (NPC) three-level inverter (3LI) enables efficient power transfer to the AC load. The NPC inverter's multi-level topology reduces switching losses and THD, leading to higher efficiency and better power quality for AC loads. In the future, we may investigate additional optimization techniques to improve the proposed system's overall effectiveness and resilience. These may include the incorporation of sophisticated control algorithms such as machine learning-based predictive

controllers or adaptive neuro-fuzzy inference systems (ANFIS) to further enhance the system's dynamic performance and robustness. Additionally, exploring novel converter topologies, such as modular multilevel converters (MMC) or interleaved converters, could address emerging challenges in the integration of renewable energy sources into the grid, improving scalability and fault tolerance. By advancing these aspects, the hybrid photovoltaic-battery energy system can achieve higher efficiency, greater reliability, and seamless integration into modern power grids, supporting the broader adoption of renewable energy technologies.

REFERENCES

[1] Zheng, J., Du, J., Wang, B., Klemeš, J.J., Liao, Q., Liang, Y. (2023). A hybrid framework for forecasting power generation of multiple renewable energy sources. Renewable and Sustainable Energy Reviews, 172: 113046. https://doi.org/10.1016/j.rser.2022.113046

[2] Peng, F., Xie, X., Wu, K., Zhao, Y., Ren, L. (2023). Online hierarchical energy management strategy for fuel cell based heavy-duty hybrid power systems aiming at collaborative performance enhancement. Energy Conversion and Management, 276: 116501. https://doi.org/10.1016/j.enconman.2022.116501

[3] Sharma, D., Jalil, M.F., Ansari, M.S., Bansal, R.C. (2023). A review of PV array reconfiguration techniques for maximum power extraction under partial shading conditions. Optik, 275: 170559. https://doi.org/10.1016/j.ijleo.2023.170559

[4] Balakishan, C., Sandeep, N., Aware, M.V. (2015). Design and implementation of three-level DC-DC converter with golden section search based MPPT for the photovoltaic applications. Advances in Power Electronics, 2015(1): 587197. https://doi.org/10.1155/2015/587197

[5] Patel, P., Yadav, A.K., Tiwari, P., Maurya, R. (2020). Performance investigation of three-level boost converter for maximum power point tracking. In 2020 IEEE Students Conference on Engineering & Systems (SCES), Prayagraj, India, pp. 1-6. https://doi.org/10.1109/SCES50439.2020.9236700

[6] Lahouar, F.E., Slama, J.B.H., Hamouda, M., Mustapha, F.B. (2014). Comparative study between two and three-level topologies of grid connected photovoltaic converters. In 2014 5th International Renewable Energy Congress (IREC), Hammamet, Tunisia, pp. 1-6. https://doi.org/10.1109/IREC.2014.6826907

[7] Zhang, Z., Zhou, H. (2019). High performance of three-level T-type grid-connected photovoltaic inverter system with three-level boost maximum power point tracking converter. Advances in Mechanical Engineering, 11(4): 1687814019843369. https://doi.org/10.1177/1687814019843369

[8] Abbassi, A., Dami, M.A., Jemli, M. (2017). A statistical approach for hybrid energy storage system sizing based on capacity distributions in an autonomous PV/Wind power generation system. Renewable Energy, 103: 81-93. https://doi.org/10.1016/j.renene.2016.11.024

[9] Benamrane, K., Abdelkrim, T., Borni, A., Benslimane, T., Abdelkhalek, O. (2016). Comparison study of two cascaded configurations of PV generators-three levels inverter for a stand-alone application in South Algeria. In 2016 4th International Conference on Control Engineering & Information Technology (CEIT), Hammamet, Tunisia, pp. 1-6. https://doi.org/10.1109/CEIT.2016.7929027

[10] Abdelkrim, T. (2010). Application du multiniveaux au filtrage actif des réseaux. Doctoral dissertation, Alger, Ecole Nationale Polytechnique.

[11] Samrat, N.H., Ahmad, N., Choudhury, I.A., Taha, Z. (2015). Technical study of a standalone photovoltaic-wind energy based hybrid power supply systems for island electrification in Malaysia. PLoS One, 10(6): e0130678. https://doi.org/10.1371/journal.pone.0130678

[12] Benlahbib, B., Bouarroudj, N., Mekhilef, S., Abdeldjalil, D., Abdelkrim, T., Bouchafaa, F. (2020). Experimental investigation of power management and control of a PV/wind/fuel cell/battery hybrid energy system microgrid. International Journal of Hydrogen Energy, 45(53): 29110-29122. https://doi.org/10.1016/j.ijhydene.2020.07.251

[13] Al-Wesabi, I., Fang, Z., Wei, Z., Dong, H. (2022). Direct sliding mode control for dynamic instabilities in DC-link voltage of standalone photovoltaic systems with a small capacitor. Electronics, 11(1): 133. https://doi.org/10.3390/electronics11010133

[14] AL-Wesabi, I., Fang, Z., Farh, H., Dagal, I., Al-Shamma'a, A., Al-Shaalan, A. (2024). Hybrid SSA-PSO based intelligent direct sliding-mode control for extracting maximum photovoltaic output power and regulating the DC-bus voltage. International Journal of Hydrogen Energy, 51: 348-370. http://doi.org/10.1016/j.ijhydene.2023.10.034

[15] Al-Ismail, F.S. (2024). A critical review on DC microgrids voltage control and power management. IEEE Access, 12: 30345-30361. http://doi.org/10.1109/ACCESS.2024.3369609

[16] Shabani, M., Dahlquist, E., Wallin, F., Yan, J. (2021). Techno-economic impacts of battery performance models and control strategies on optimal design of a grid-connected PV system. Energy Conversion and Management, 245: 114617. https://doi.org/10.1016/j.enconman.2021.114617

[17] Bahri, A., Thameur, A., Mordjaoui, M., Bechouat, M., Sedraoui, M. (2021). An optimal tilt integral derivative applied to the regulation of DC link voltage in a stand-alone hybrid energy system. Journal Européen des Systèmes Automatisés, 54(4): 607-616. https://doi.org/10.18280/jesa.540410

[18] Bahri, A., Mezhoud, N., Benamrane, K., Ayachi, B., Abdelkrim, T., Bechouat, M. (2023). Fuzzy logic MPPT controller for a standalone PV/battery hybrid energy system. Algerian Journal of Renewable Energy and Sustainable Development, 5(2): 227-239.

[19] Gada, S., Fekik, A., Mahdal, M., Vaidyanathan, S., Maidi, A., Bouhedda, A. (2023). Improving power quality in grid-connected photovoltaic systems: A comparative analysis of model predictive control in three-level and two-level inverters. Sensors, 23(18): 7901. https://doi.org/10.3390/s23187901

[20] Bahri, A. (2017). Modélisation et simulation d'un générateur photovoltaïque sous Matlab/Simulink Etude pratique site Oued Nechou à Ghardaïa. El-Wahat Journal for Research and Studies, 10(1): 1-19.

[21] Benamrane, K., Abdelkrim, T., Benlahbib, B., Bouarroudj, N., Borni, A., Lakhdari, A., Bahri, A.

(2021). New optimized control of cascaded multilevel converters for grid tied photovoltaic power generation. Journal Européen des Systèmes Automatisés, 54(5): 769-776. https://doi.org/10.18280/jesa.540512

[22] Tian, J., Qu, J., Zhao, F., Chen, X., Wang, Y., Gan, Y. (2023). Topology analysis and parameter design of three-level multi-input DC/DC converter based on multi-source access. Archives of Electrical Engineering, 72(1): 59-80. https://doi.org/10.24425/aee.2023.143690

[23] Abdullah, R., Rahim, N.A., Raihan, S.R.S., Ahmad, A.Z. (2014). Five-level diode-clamped inverter with three-level boost converter. IEEE Transactions on Industrial Electronics, 61(10): 5155-5163. https://doi.org/10.1109/TIE.2013.2297315

[24] Singh, S., Lee, D.C., Ho, A.V. (2023). Active impedance network buck-boost three-level T-type inverter with enhanced voltage gain. IEEE Access, 11: 8005-8016. https://doi.org/10.1109/ACCESS.2023.3238718

[25] Feloups, C.E., Ali, A.I., Mohamed, E.E. (2018). Single-phase seven-level PWM inverter for PV systems employing multi-level boost converter. In 2018 International Conference on Innovative Trends in Computer Engineering (ITCE), Aswan, Egypt, pp. 403-409. https://doi.org/10.1109/ITCE.2018.8316658

[26] Borni, A., Bouarroudj, N., Bouchakour, A., Zaghba, L. (2017). P&O-PI and fuzzy-PI MPPT Controllers and their time domain optimization using PSO and GA for grid-connected photovoltaic system: A comparative study. International Journal of Power Electronics, 8(4): 300-322. https://doi.org/10.1504/IJPELEC.2017.085199

[27] Dwaza, K., Krishnamurthy, S. (2024). Application perturb and observe maximum power point tracking technique for CubeSat power systems. In 2024 32nd Southern African Universities Power Engineering Conference (SAUPEC), Stellenbosch, South Africa, pp. 1-5. https://doi.org/10.1109/SAUPEC60914.2024.10445093

[28] Abdelkrim, T., Benamrane, K., Benslimane, T., Abdelkhalek, O., Borni, A. (2017). Stability study of output voltages of two-stage PV system based three levels inverter. Energy Procedia, 139: 658-663. https://doi.org/10.1016/j.egypro.2017.11.268

[29] Wang, Y., Tian, J., Sun, Z., Wang, L., Xu, R., Li, M., Chen, Z. (2020). A comprehensive review of battery modeling and state estimation approaches for advanced battery management systems. Renewable and Sustainable Energy Reviews, 131: 110015. https://doi.org/10.1016/j.rser.2020.110015

[30] Zhou, W., Zheng, Y., Pan, Z., Lu, Q. (2021). Review on the battery model and SOC estimation method. Processes, 9(9): 1685. https://doi.org/10.3390/pr9091685

[31] Koulali, M., Berkani, A., Negadi, K., Mankour, M., Mezouar, A. (2020). Sliding fuzzy controller for energy management of residential load by multi-sources power system using wind PV and battery. Journal Européen des Systèmes Automatisés, 53(3): 305-315. https://doi.org/10.18280/jesa.530301

[32] Chong, L.W., Wong, Y.W., Rajkumar, R.K., Isa, D. (2018). An adaptive learning control strategy for standalone PV system with battery-supercapacitor hybrid energy storage system. Journal of Power Sources, 394: 35-49. https://doi.org/10.1016/j.jpowsour.2018.05.041

[33] Pu, Q., Zhu, X., Liu, J., Cai, D., et al. (2020). Integrated optimal design of speed profile and fuzzy PID controller for train with multifactor consideration. IEEE Access, 8: 152146-152160. https://doi.org/10.1109/ACCESS.2020.3017193

[34] Sharma, K., Palwalia, D.K. (2017). A modified PID control with adaptive fuzzy controller applied to DC motor. In 2017 International Conference on Information, Communication, Instrumentation and Control (ICICIC), Indore, India, pp. 1-6. https://doi.org/10.1109/ICOMICON.2017.8279151

[35] Baramadeh, M.Y., Abouelela, M.A.A., Alghuwainem, S.M. (2021). Maximum power point tracker controller using fuzzy logic control with battery load for photovoltaics systems. Smart Grid and Renewable Energy, 12(10): 163-181. https://doi.org/10.4236/sgre.2021.1210010

[36] Rai, N., Rai, B. (2018). Control of fuzzy logic based PV-battery hybrid system for stand-alone DC applications. Journal of Electrical Systems and Information Technology, 5(2): 135-143. https://doi.org/10.1016/j.jesit.2018.02.007

[37] Elkhateb, A., Abd Rahim, N., Selvaraj, J., Uddin, M.N. (2014). Fuzzy-logic-controller-based SEPIC converter for maximum power point tracking. IEEE Transactions on Industry Applications, 50(4): 2349-2358. https://doi.org/10.1109/TIA.2014.2298558

[38] Chauhan, S., Singh, B. (2021). Control of solar PV-integrated battery energy storage system for rural area application. IET Renewable Power Generation, 15(5): 1030-1045. https://doi.org/10.1049/rpg2.12086

[39] Kalla, U.K., Kaushik, H., Singh, B., Kumar, S. (2019). Adaptive control of voltage source converter based scheme for power quality improved grid-interactive solar PV–battery system. IEEE Transactions on Industry Applications, 56(1): 787-799. https://doi.org/10.1109/TIA.2019.2947397

[40] Raju, B.S., Babu, K.S., Azam, S.G. (2015). Fractional order PID control for solar PV and battery storage systems using three-level NPC inverter. International Journal of Scientific Engineering and Technology Research, 4(40): 8672-8681.